

Fermi surface of a ferrooxypnictide superconductor determined by quantum oscillations.

A.I. Coldea¹, J.D. Fletcher¹, A. Carrington¹, J.G. Analytis², A.F. Bangura¹, J.-H. Chu²,
A. S. Erickson², I.R. Fisher², N.E. Hussey¹, and R.D. McDonald³

¹*H. H. Wills Physics Laboratory, Bristol University, Tyndall Avenue, BS8 1TL, United Kingdom*

²*Geballe Laboratory for Advanced Materials and Department of Applied Physics, Stanford University, Stanford, California 94305-4045, USA*

³*National High Magnetic Field Laboratory, Los Alamos National Laboratory, MS E536, Los Alamos, New Mexico 87545, USA*

The recent discovery^{1,2} of superconductivity in ferrooxypnictides, which have a maximum transition temperature intermediate between the two other known high temperature superconductors MgB₂ and the cuprate family, has generated huge interest and excitement. The most critical issue is the origin of the pairing mechanism. Whereas superconductivity in MgB₂ has been shown to arise from strong electron-phonon coupling³, the pairing glue in cuprate superconductors is thought by many to have a magnetic origin⁴. The oxypnictides are highly susceptible to magnetic instabilities^{5,6}, prompting analogies with cuprate superconductivity⁷. Progress on formulating the correct theory of superconductivity in these materials will be greatly aided by a detailed knowledge of the Fermi surface parameters. Here we report for the first time extensive measurements of quantum oscillations in a Fe-based superconductor, LaFePO, that provide a precise calliper of the size and shape of the Fermi surface and the effective masses of the relevant charge carriers. Our results show that the Fermi surface is composed of nearly-nested electron and hole pockets in broad agreement with the band-structure predictions but with significant enhancement of the quasiparticle masses. The correspondence in the electron and hole Fermi surface areas provides firm experimental evidence that LaFePO, whilst unreconstructed, lies extremely close to a spin-density-wave instability, thus favouring models that invoke such a magnetic origin for high-temperature superconductivity in oxypnictides.

LaFePO was the first of the ferrooxypnictide superconductors to be discovered and has a transition temperature of $T_c \sim 7$ K¹. Substituting the pnictogen P for As results in the isostructural compound LaFeAsO, which is in its undoped state is non-superconducting and has a spin-density wave ground state. With a small amount of electron doping it becomes a relatively high- T_c superconductor ($T_c \sim 25$ K). Of the other compounds in this series the highest T_c found so far is 55K for SmFeAsO_{1-x}F_x (Ref 2). Calculations⁵ suggest that the conventional electron-phonon coupling mechanism is too weak to stabilize such a high- T_c state in these materials; instead several authors have suggesting a magnetic fluctuation mediated pairing mechanism. Theoretical models of unconventional pairing mechanisms rely on a detailed knowledge of the Fermi surface topology and the strength of the coupling of the quasiparticles to excitations; of particular importance for the ferro-oxypnictides is the degree to which the Fermi surface is nested^{5,6,8}.

For several decades the study of quantum oscillations has proved to be a powerful probe of Fermi surface parameters. For example, the recent observation of quantum oscillations in both underdoped and overdoped high temperature cuprate superconductors has produced a marked change in our understanding of these materials⁹⁻¹¹. Its usefulness stems from the fact that it is a three-dimensional bulk probe which is extremely precise; the size of the Fermi surface cross-sections can typically be measured to an accuracy of 0.05 % of the area of the first Brillouin zone. Furthermore, this technique is not affected by surface effects which can sometimes considerably complicate the interpretation of other relevant techniques such as angle resolved photoemission spectroscopy (ARPES). The main experimental difficulties with observing quantum oscillations are that the samples must be extremely clean and the upper critical field must be low enough for the normal state to be accessed; LaFePO is a material which fulfils both these requirements. We have succeeded to grow single crystals with residual resistance ratios of up to 90, which show bulk superconductivity ($T_c \sim 6.3$ K) and have an upper critical field of 0.68 T for $\mathbf{B} \parallel c$ (7.2 T for $\mathbf{B} \perp c$).

Fig. 1a shows raw torque measurements versus magnetic field at low temperatures ($T = 0.35$ K) measured on a small single crystal sample. At low fields the torque signature of a bulk anisotropic type-II superconductor is observed (a dome-shaped feature with a kink at H_{c2}). This is almost perfectly reversible, indicating weak pinning of vortices. A superconducting transition is seen at $\mu_0 H_{c2} = 5.6$ T in the data, where the magnetic field is almost parallel to the ab plane. This feature moves to lower field as the sample is rotated towards $\mathbf{B} \parallel c$. For magnetic field above approximately 9 T oscillations, periodic in inverse field, are clearly visible. These arise from the de Haas van Alphen (dHvA) effect and become more pronounced after subtraction of a monotonic background (Figs. 1b). A similar periodic oscillation in the c -axis resistance of another sample arising from the related Shubnikov-de Haas effect is shown in Fig 1c. As the signals are comprised of a superposition of several oscillatory components the data are most easily understood by taking the fast Fourier transform (FFT) as shown in Figs. 1d and 1e. The peaks in these spectra correspond to the dHvA frequencies F which are related to the extremal cross-sectional areas A_k , of the Fermi surface via the Onsager relation, $F = (\hbar/2\pi e) A_k$. The evolution of the dHvA frequencies as the magnetic field is rotated from being parallel to c ($\theta = 0^\circ$) towards the ab plane ($\theta = 90^\circ$), allows us to construct a detailed three dimensional picture of the shape and size of the Fermi surface. Four frequencies have significantly larger

amplitudes than the others; we name the first, closely split, pair of frequencies α_1 and α_2 ($F \sim 1$ kT, $\Delta F \sim 40$ T for $\theta=0$) and the two higher frequencies, β_1 and β_2 (1.9 kT and 2.4 kT for $\theta=0$). Besides these intense features (and their harmonics), we also see several other frequencies of smaller amplitude, which we label γ , δ , ϵ and η . The observed frequencies represent a fraction varying between 2.8% to 9 % of basal plane area of the Brillouin zone. They are significantly larger than those observed in the double-layer Fe-As compound, SrFe₂As₂¹², which is non-superconducting, and is likely to have a reconstructed Fermi surface at low temperatures due to the spin-density-wave ground state.

Fig. 1e and 2a show the strong angular dependence of the main frequencies as well as a significant variation of their amplitudes. For a purely two-dimensional Fermi surface the dHvA frequency should vary like $1/\cos \theta$. All of the observed frequencies observed near $\mathbf{B}||c$ approximately follow this behaviour. Deviations from this, indicating the degree of warping of the quasi-two-dimensional cylinder, are shown by plotting $F \cos \theta$ as in Fig 2c. It can be seen that the β orbits originate from a section of FS which has significantly warping whereas for the α orbit FS sheet the warping is much smaller. The detailed angle dependence of the β orbits is well described by Yamaji's model of simple cosine warping of a two-dimensional cylinder¹³. As expected we observe a large increase in the amplitude of the β oscillations at $\theta \sim 45^\circ$, where the two frequencies cross.

The cyclotron effective mass of the quasiparticles on the various orbits were determined by fitting the temperature dependent amplitude of the oscillations to the conventional Lifshitz-Kosevich formula,¹⁴ as shown in Fig. 2c. These measurements were made with the field close to the c -axis and the value for $\theta=0^\circ$ was inferred using the usual approximation that the mass scales with the dHvA frequency. The obtained masses range between $1.7 m_e$ and $2.1 m_e$, where m_e is the mass of a free electron (see Table 1).

We now compare our experimental observations with predictions from density functional theory band structure calculations¹⁵. Our calculated Fermi surface, based on experimental lattice parameters and atomic positions, is in excellent agreement with that reported by Lebègue¹⁶; the bands crossing the Fermi level are derived mainly from the Fe orbitals. It comprises of small, slightly warped tubular sections of Fermi surface running along the crystallographic c direction. There are two hole sheets centred on the Brillouin zone centre Γ and two electron sheets centred at the zone corner M (see Fig. 3c). In addition, there is a small three-dimensional hole pocket centred on Z.

The dHvA extremal orbit frequencies calculated from this Fermi surface are shown alongside the experimental data in Fig. 3a. The calculation predicts that there should be 9 frequencies for θ close to zero (two for each tube plus one for the 3D hole pocket) in the range 1-3 kT. As shown in Fig. 3a, this is broadly similar to what is observed experimentally. In particular orbits β_1 and β_2 closely resemble those expected

from the larger electron cylinder in both frequency and curvature. The shape and splitting of orbits α_1 and α_2 closely match the smaller electron cylinder. This assignment is further supported by the much larger amplitude of these oscillations, which indicate that they suffer significantly less damping (we estimate a mean free path of $\sim 1300\text{\AA}$ for the α orbits and 800\AA for the β orbits). This is a natural consequence of the fact that both of these orbits originate from the same piece of Fermi surface in the larger unfolded Brillouin zone (corresponding to the Fe-sublattice). The three remaining frequencies (ϵ , γ , δ) then correspond to hole orbits, although their exact assignment is less clear. As the dHvA torque is proportional to $dF/d\theta$, the predicted weak variation of $F(\theta)$ for $\theta \sim 0$ for the maximum frequencies of band 2 and 3, could make these frequencies difficult to observe experimentally leaving only the two minimum areas from these sheets plus the 3D pocket. Note that the η orbit was only observed in one sample (measured up to 18 T) and we cannot rule out the possibility this weak signal originates from a small misaligned piece of crystal.

In order to superimpose the experimental data with the calculated orbits it is necessary to shift the energies of each band slightly. Agreement with the electron orbits α_1 , α_2 , β_1 and β_2 is improved with band shifts of -20 and +83 meV respectively. Applying a uniform shift of +50meV to the other bands results in good agreement for the minima of band 2 with the γ orbit and the frequencies expected from band 3 are within 20-30% of orbits δ and ϵ . The Fermi surface produced by this procedure is shown in Figs. 3c-g.

As in the other ferroxyptictides, in LaFePO the bandstructure is very sensitive to the position of the P atom⁶. The calculations predict that the equilibrium position of P is around 0.05 Å away from its experimental one¹⁷, perhaps because the effect of magnetic fluctuations have not been included¹⁷. A calculation of the bandstructure with the P atom in this relaxed structure results in hole orbits which are much too small to explain our data and much larger band energy shifts are needed to bring it into even approximate agreement. In contrast, a previous ARPES study of the Fermi surface of LaFePO¹⁸ has showed bands which are consistent with the bandstructure calculated with the relaxed structure with all bands shifted up by 55 meV and renormalized by a factor of 2. Although this shift is similar in magnitude to that applied here, the use of the relaxed structure means that the Fermi surface cross-sections are considerably different to those we measure. For example, the APRES results indicate a hole sheet which has a crosssection equivalent to a dHvA frequency of ~ 12 kT which is ~ 7 times larger than we find from our results. It is expected that for undoped LaFePO the volume of the electron and hole sheets should be equal. For our shifted bands the imbalance is 0.08 electrons per unit cell whereas the ARPES results imply an imbalance of around 1 electron per unit cell, suggesting significant doping of the surface layer¹⁸.

The band structure calculation allows us to estimate the many body (electron-phonon and electron-electron) enhancements of the quasiparticle masses over their band values. Note that for the observed orbits the band masses do not depend strongly on the shift applied. The renormalized factor $(1+\lambda) = m^*/m_b$, for

the various orbits are listed in Table 1. For the electron bands a substantial renormalisation is found, with $(1+\lambda)$ lying in the range 2-3. For the electron orbits a calculation of λ is difficult as the calculated frequencies do not correspond exactly to the experimental ones – however as the band masses are all in the range $0.5-1 m_e$ and the measured m^* values are $\sim 2 m_e$ it is reasonable to deduce a similar level of enhancement. Estimates of the measured electronic specific heat coefficient (γ) vary between $7-12 \text{ mJ/mol K}^2$ ¹⁹⁻²¹ whereas the value obtained from our calculations is 5.6 mJ/mol K^2 . Hence, our orbit-specific renormalisations are consistent with the global renormalisation estimated from specific heat data as well as ARPES measurements¹⁶.

A two-dimensional cut of our calculated Fermi surface at $k_z=0$ and $k_z=\pi/c$ is shown in Figs. 3f and 3g. It can be seen that hole pockets at the corner of the Brillouin zone (BZ) are almost identical in shape and size to the electron pockets at the centre of the zone, equivalent to a inter-band nesting vector $\mathbf{Q} \sim [\pi, \pi, 0]$. In fact, the similarity in areas of the electron and hole pockets can be inferred directly from the correspondence between the dHvA frequencies for the electron and hole pockets. Such near (but not perfect) nesting is an essential ingredient to theories of the superconductivity in the ferroxypticide superconductors^{5,8,22} based on spin-fluctuations.

Samples and Experimental methods

Single crystals of LaFePO, with dimensions up to $0.2 \times 0.2 \times 0.04 \text{ mm}^3$, were grown from a tin flux using modified conditions from those described by Zimmer et al.²³ Structural refinements based on single crystal x-ray diffraction (on crystals from the same batch) indicate full occupancy for all sites (to an accuracy of $\sim 2\%$ for the oxygen). The lattice parameters and La/P positions were found to be $a = 3.941 \text{ \AA}$, $c = 8.507 \text{ \AA}$, and the $z_{\text{La}}=0.1489$, $z_{\text{P}}=0.63477$ in agreement with previous results.¹ Torque measurements were performed with a piezoresistive microcantilever down to 0.3 K on different single crystals from the same batch, one in Bristol (sample B) up to 18 T and at another crystal at the NHMFL, Tallahassee, (sample A) up to 45 T . Interplane electrical transport has been measured on a third sample (sample C). Measurements were performed in He^3 liquid with an error in the temperature $<0.1 \text{ K}$ in Bristol or in He^3 liquid/vapour with an error of $<0.2 \text{ K}$ in Tallahassee. A rotating sample holder allowed the angle θ between the magnetic field direction and the c axis to be varied. For sample B the platform angle was measured with a pick-up coil (using a small modulated magnetic field collinear with the main field) with an uncertainty of $<1^\circ$. For sample A changes of platform angle are inferred from the gearing mechanism of the rotator with an accuracy of $\pm 2^\circ$. In both cases the relative orientation of the crystal was deduced from the symmetry of the torque signal (using the dHvA frequency or H_{c2}). The variation of the piezoresistance of the cantilever is measured with a Wheatstone bridge with an ac excitation at a frequency of 72 Hz . At 40 T , the oscillatory part of torque is typically 20% of the background torque. The sensitivity of cantilevers of this type is approximately 0.1 degree per Ohm. At certain angles and at the

highest fields, the deflection of the cantilever is large enough to generate harmonics of the main dHvA frequencies, which are indicated where present. We exclude the possibility of observing any signal from possible tin inclusions as the expected masses for tin are much lower ($< 0.7 m_e$) than we observe²⁴. In addition, the symmetry of the dHvA signal is also found to be identical with that due to superconductivity. Bandstructure calculations we performed using the WIEN2K code, using 10^4 k points (in the full Brillouin zone) for convergence and 10^5 k points for the Fermi surface calculations¹⁵.

References

1. Kamihara, Y. *et al.* Iron-based layered superconductor: LaFePO. *J. Am. Chem. Soc.* **128**, 10012-10013 (2006).
2. Ren, Z.-A. *et al.*, Superconductivity at 55 K in iron-based F-doped layered quaternary compound $\text{Sm}[\text{O}_{1-x}\text{F}_x]\text{FeAs}$. *Chin. Phys. Lett.* **25**, 2215-2216 (2008).
3. Mazin, I. I. and Antropov, V. P. Electronic structure, electron-phonon coupling, and multiband effects in MgB_2 . *Physica C*, **385**, 49-65 (2003).
4. Maier, T. A. *et al.* Dynamics of the Pairing Interaction in the Hubbard and t - J Models of High-Temperature Superconductors, *Phys. Rev. Lett.* **100**, 237001 (2008); and references therein.
5. Mazin I.I., *et al.*, Unconventional sign-reversing superconductivity in LaFeAsO $_{1-x}$ F $_x$, arXiv: 0803.2740v3;
6. Bangura, A. F. *et al.*, The challenge of unravelling magnetic properties in LaFeAsO arXiv: 0806.1869.
7. Si Q and Abrahams E., Strong Correlations and Magnetic Frustration in the High T_c Iron Pnictides arXiv:0804.2480.
8. Chubukov, A.V., Efremov, D., Eremin, I. Magnetism, superconductivity, and pairing symmetry in Fe-based superconductors, arXiv:0807.37355.
9. Doiron-Leyraud, N. *et al.* Quantum oscillations and the Fermi surface in an underdoped high- T_c superconductor, *Nature* **447**, 565 (2007).
10. Bangura, A. F. *et al.* Small Fermi Surface Pockets in Underdoped High Temperature Superconductors: Observation of Shubnikov-de Haas Oscillations in $\text{YBa}_2\text{Cu}_3\text{O}_8$, *Phys. Rev. Lett.* **100**, 0470041-4 (2008).
11. Vignolle *et al.*, Quantum oscillations in an overdoped high temperature Superconductor, to appear in *Nature* (2008).
12. Sebastian, S.E. *et al.*, Quantum oscillations in the undoped parent magnetic phase of a high temperature superconductor, arXiv:0806.4726.
13. Yamajiri, K. On the angle dependence of the magnetoresistance in quasi-two-dimensional organic superconductors, *J. Phys. Soc. Japan*, **58**, 1520-1523 (1989).
14. Shoenberg, D. *Magnetic oscillations in metals* (Cambridge University Press, Cambridge 1984).
15. Blaha, P *et al.*, WIEN2K, an augmented plane wave + local orbitals program for calculating crystal properties, Karlheinz Schwarz, Technica Universität Wien, Austria, (2001).
16. Lebègue, S., Electronic structure and properties of the Fermi surface of the superconductor LaFePO. *Phys. Rev. B* **75**, 035111-0351115 (2007).
17. Mazin, II and Johannes, M.D. A key role for unusual spin dynamics in ferroptictides, arXiv:0807.3737.
18. Lu, D.H. *et al.*, Electronic structure of the iron-based superconductor LaFePO, arXiv:0807.2009.
19. Analytis, J. *et al.*, (unpublished).
20. Kohama, Y. *et al.*, Possible unconventional superconductivity in iron-based layered compound LaFePO: Study of heat capacity, arXiv:0806.3139.
21. McQueen, T.M. *et al.*, Intrinsic properties of stoichiometric LaOFeP, arXiv:0805.2149.
22. Bang Y., and Cho, H.-Y. Possible pairing states of the Fe-based superconductors, arXiv:0807.3912.
23. Zimmer, B. I. *et al.*, The rare earth transition metal phosphide oxides LnFePO, LnRuPO and LnCoPO with ZrCuSiAs type structure. *J. Alloy. Comp.* **229**, 238–242 (1995).
24. Craven J.E., Band Structure and Fermi surface of white tin as derived from de Haas van Alphen data, *Phys. Rev.* **182**, 693-704 (1969).

Acknowledgements

We thank E.A. Yelland for sharing code to calculate dHvA parameters from the results of bandstructure calculations, N. Fox for the preparation of Hall probes and MF Haddow for X-ray diffraction and I. Mazin for helpful comments regarding the bandstructure. This work was supported financially by EPSRC

(UK). AIC is grateful to the Royal Society for a Dorothy Hodgkin Royal Society Fellowship and financial support. Work at Stanford supported by the Department of Energy, Office of Basic Energy Sciences under contract DE-AC02-76SF00515. A portion of this work was performed at the National High Magnetic Field Laboratory in Tallahassee, Florida, which is supported by NSF Cooperative Agreement No. DMR-0654118, by the State of Florida, and by the DOE.

Author Information

The authors declare no competing financial interests. Correspondence and request for materials should be addressed to Amalia Coldea (amalia.coldea@bristol.ac.uk) or Antony Carrington (a.carrington@bristol.ac.uk).

Orbit	F($\theta=0$) (kT)	Sample A		Sample B		Calc m_b/m_e
		m^*	(1+ λ)	m^*	(1+ λ)	
α_1	0.985(7)	1.9(2)	2.5(2)	1.8(1)	2.4(2)	0.76
α_2	1.025(7)	1.9(2)	2.4(2)	1.8(1)	2.3(2)	0.80
β_1	1.91(1)	1.7(2)	2.6(3)	1.8(1)	2.6(2)	0.67
β_2	2.41(1)	1.8(2)	2.1(3)	1.9(1)	2.1(2)	0.89
δ	1.36(2)	1.8(3)				
γ	0.73(2)	1.7(3)				
ε	1.69(2)	2.1(3)				

Table 1: Band masses and measured effective masses for the observed orbits for LaFePO. m_b is the band-mass estimated from the bandstructure calculations, and $(1+\lambda) = m^*/m_b$ is the calculated mass enhancement.

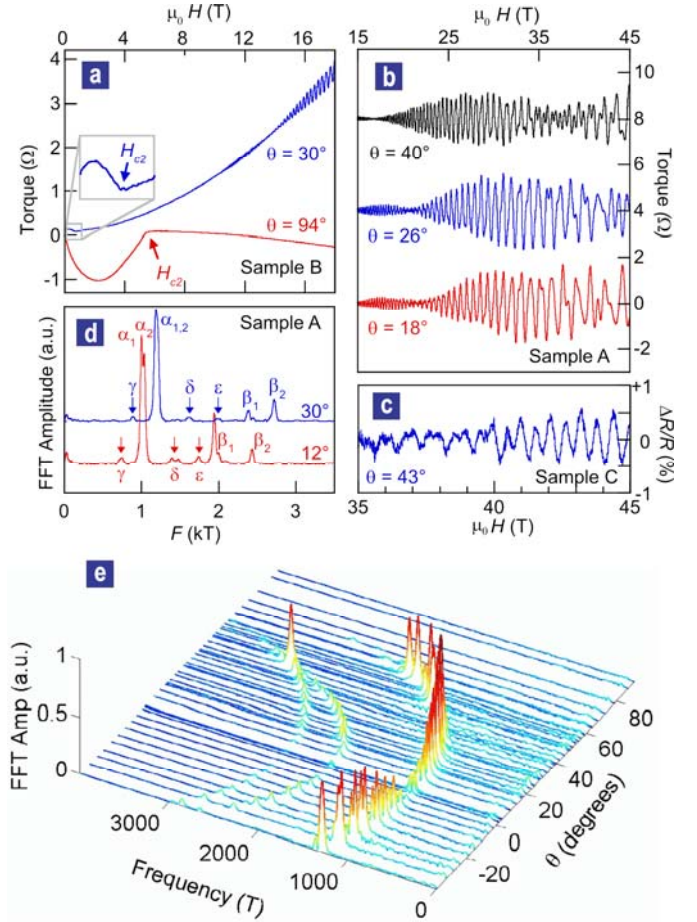


Figure 1. Quantum oscillations in LaFePO. **a.** Torque measurements on LaFePO measured at $T = 0.35$ K and in magnetic fields up to 18 T for different orientations θ (angle between the magnetic field and the c axis) for sample B. Units are of lever resistance (1Ω corresponds to a lever deflection of $\sim 0.1^\circ$). The enlarged region shows $\mu_0 H_{c2} = 0.7$ T. **b.** dHvA in sample A obtained by measuring torque in magnetic fields up to 45 T. A 5th order polynomial has been subtracted to remove the non-oscillatory background and the curves are offset for clarity. **c.** Resistance oscillations (SdH) at high field in sample C (background subtracted as above). **d.** Fourier transform spectra using a field window between 15-45 T for two different orientations in magnetic field (sample A). **e.** The angle dependence of the Fourier transform using a field window between 10-18 T showing the angle dependence of the frequency and amplitude of the oscillations (sample B). The large peak near 45 is due to the enhancement of the dHvA at the ‘Yamaji Angle’ (see text).

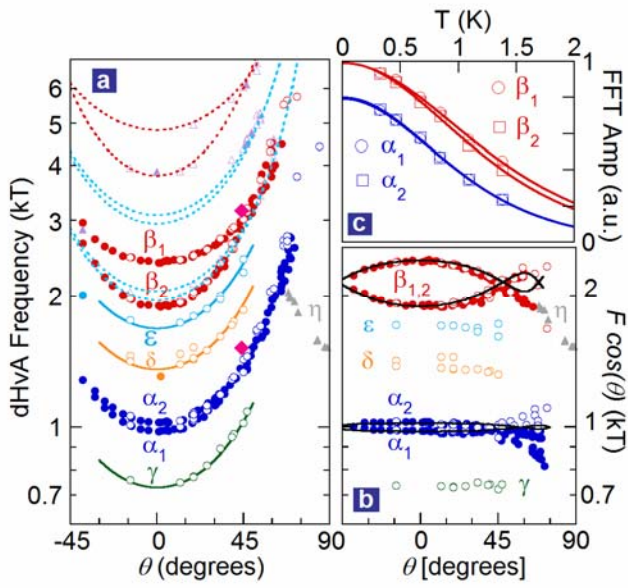


Figure 2. Fermi surface parameters. **a** Angular dependence of all observed frequencies found experimentally. Sample A is represented by open symbols, sample B by closed symbols and diamond symbols correspond to sample C. Solid lines are fits to $1/\cos(\theta)$ behaviour expected for a two-dimensional Fermi surface cylinder. Suspected harmonics are shown with triangles. Dashed lines represent expected location of harmonics of α_1 , α_2 , β_1 and β_2 . Very good agreement between crystals is found for the main branches α and β . The branches δ , ϵ and γ were only clearly seen in sample A, probably because this was measured in a significant higher magnetic field (up to 45 T), which overcomes the damping produced by impurity scattering. An eighth branch η was seen for sample A only, when the field was aligned close to the ab plane. **c** A plot of $F \cos(\theta)$ reveals deviations from the two-dimensional angle dependence due to corrugation of the quasi-2D tubes, which is more pronounced for orbits β_1 and β_2 . Solid lines show the behaviour expected from a simple warping. **b** Variation with temperature of the Fourier amplitude along with a fit to the standard Lifshitz-Kosevich formula used to extract the effective mass. Representative data from sample B at an angle of $\theta=32^\circ$ is shown for an FFT over the range 10-17.9 T for α orbits and 15-17.9 T for β orbits. Data are offset for clarity. Mass values are reported in Table 1.

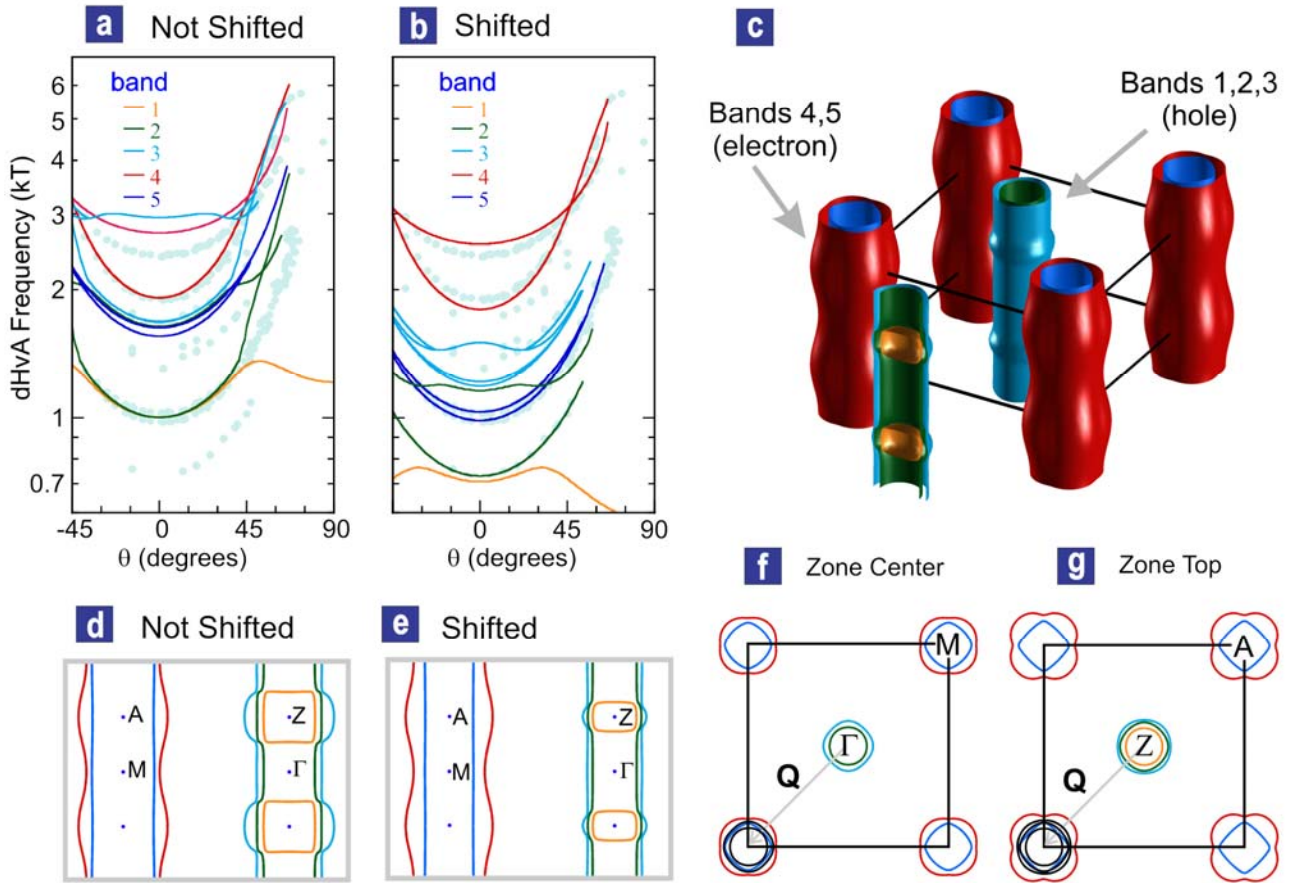


Figure 3. Comparison of the experimental and calculated Fermi surface of LaFePO. **a**, Angle dependence of the dHva frequencies predicted by bandstructure calculations using experimental lattice parameters and atomic positions

(the experimental points from figure 2a are shown in grey – harmonics and uncertain points have been omitted). **b**, As in a) but with the band energies adjusted as described in the text. **c**, A three-dimensional representation of the calculated Fermi surface of LaFePO (after band shifts have been applied). The solid black lines indicate the first Brillouin zone. **d**, Two dimensional (110) cut of the Fermi surface calculated with the non-shifted bands showing the c-axis warping of the Fermi surface. The symmetry labels of the BZ are shown. **e**, as for d) but with the shifted bands. **f**, Two dimension (001) cut of the Fermi surface at the centre of the BZ (Γ XM plane) showing the degree of nesting between the electron and hole pockets (indicated by the grey arrow). **g**, as f) but for a cut at the top of the BZ (ZAR plane).